Applied Catalysis B: Environmental 196 (2016) 174–184

Contents lists available at ScienceDirect

Applied Catalysis B: Environmental

journal homepage: www.elsevier.com/locate/apcatb

Shape evolution of carbon supported Pt nanoparticles: From synthesis to application

Mila N. Krstajić Pajić[a], Sanja I. Stevanović[a], Vuk V. Radmilović[b], Aleksandra Gavrilović-Wohlmuther[c], Velimir R. Radmilović[d,e], Snežana Lj. Gojković[d], Vladislava M. Jovanović[a,*]

[a] Department of Electrochemistry, ICTM, University of Belgrade, Njegoševa 12, 11000 Belgrade, Serbia
[b] Innovation Center, Faculty of Technology and Metallurgy, University of Belgrade, Karnegijeva 4, 11000 Belgrade, Serbia
[c] CEST-Centre of Electrochemical Surface Technology GmbH, Viktor-Kaplan Strasse 2, 2700 Wiener Neustadt, Austria
[d] Faculty of Technology and Metallurgy, University of Belgrade, Karnegijeva 4, 11000 Belgrade, Serbia
[e] Serbian Academy of Sciences and Arts, Knez Mihailova 35, 11000 Belgrade, Serbia

ARTICLE INFO

Article history:
Received 14 March 2016
Received in revised form 10 May 2016
Accepted 16 May 2016
Available online 17 May 2016

Keywords:
Cuboidal Pt particles
Formic acid oxidation
CO oxidation

ABSTRACT

In this research, a water-in-oil microemulsion method with HCl as a capping agent was applied to synthesize carbon supported Pt catalysts. Varying the concentration of HCl caused changes in the shape of obtained nanoparticles, i.e. preferential growth of certain facets. Addition of catalyst support in the synthesis process facilitated the cleaning procedures necessary to remove the surfactant residues. Prepared catalyst powders were characterized by X-ray diffraction (XRD) and transmission electron microscopy (TEM). XRD analysis indicated the influence of HCl addition on the crystallite size and crystal habit. TEM revealed that addition of higher amounts of the capping agent led to the formation of a noticable amount of particles with concave cubic or branched-like structures. Influence of the catalyst particles shape on its electrochemical properties was tested in the oxidations of CO_{ads}, ammonia and formic acid. The latter one was examined in terms of both activity and stability of *as prepared* and oxide-annealed (electrochemically treated) catalysts. The results clearly demonstrate that even small changes in the nanoparticle surface structure give rise to distinct modifications in their properties. Concave cubic particles, in comparison to other catalysts, show improved catalytic properties and the contribution of their preferentially oriented {100} facets is electrochemically detectable.

1. Introduction

Oxidation of carbon monoxide and oxidation of formic acid are among the most intensively studied reactions on Pt, from both fundamental and a technical point of view. Being the simplest reactions, they are models for studying the oxidation of small organic molecules (SOMs) in which CO usually appears as poisoning intermediate. On the other hand, SOMs like formic acid or methanol are potential fuels for polymer electrolyte fuel cells. This possibility has actually intensified the examinations of these reactions in the search for active and CO tolerant Pt based catalysts. However, it is important to note that both of these reactions are sensitive to the structure of the Pt surface.

Oxidation of adsorbed CO proceeds through a Langmuir-Hinshelwood mechanism, i.e. CO_{ads} reacts with OH_{ads} species [1]. This is an extremely structure sensitive reaction and can be used as a fingerprint of the surface morphology [2]. Studies of the reaction on different single crystal stepped surfaces, consisting of the monoatomic steps allocated between the terraces of different lenght, indicated that such surface sensitivity should be associated with the adsorption of OH species on the surface defects (steps) [3]. As the density of the steps present on these surfaces increases, the CO oxidation peak shifts to more negative potentials [4]. Results obtained on low-index Pt single crystals have shown that two different forms of CO_{ads} are mustered and oxidized in two potential regions [5]. Weakly adsorbed state is oxidized at lower potentials in the pre-ignition region, while strongly adsorbed CO is oxidized at higher potentials in the ignition region. The activity of low-index single crystals for the reaction in pre-ignition region is in order: Pt(110) < Pt(111) < Pt(100), while at the ignition potentials the order is opposite. Further studies on these surfaces have

* Corresponding author.
E-mail address: vlad@tmf.bg.ac.rs (V.M. Jovanović).

http://dx.doi.org/10.1016/j.apcatb.2016.05.033
0926-3373/

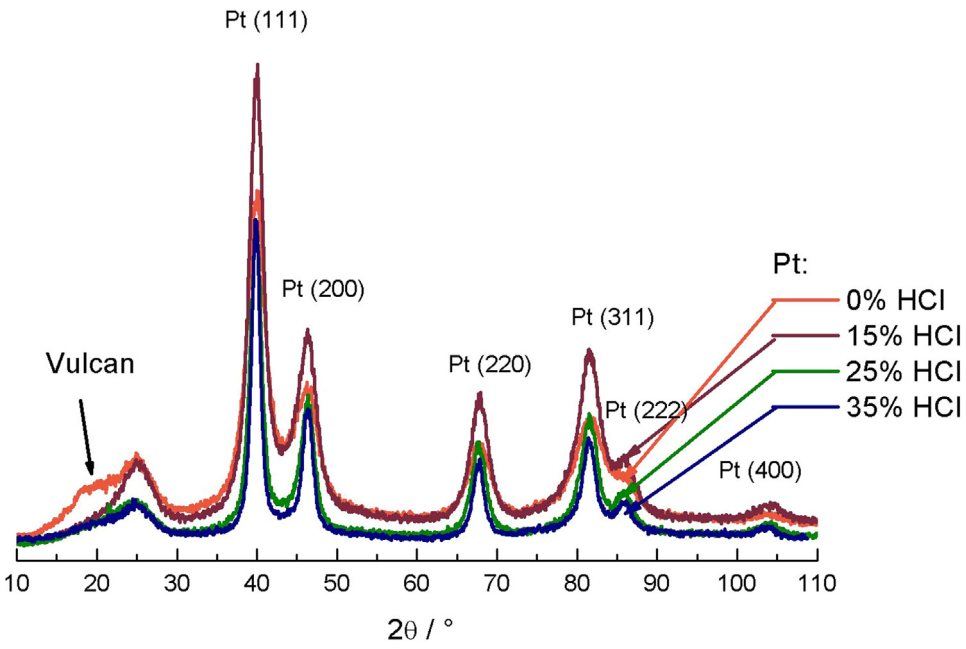

Fig. 1. XRD patterns of the supported Pt/C catalysts.

revealed that the under-coordinated atoms on Pt ad-islands are responsible for the CO oxidation in the pre-ignition region, since the reaction proceeds through only one peak on the surface free of these ad-islands, i.e. on the surface electrochemically treated up to the potentials of Pt oxide formation [2].

On the other hand, formic acid oxidation on Pt electrodes follows the dual path mechanism [6] involving a reactive intermediate (main path – dehydrogenation) and adsorbed CO as a poisoning species (parallel path – dehydratation), both generating CO_2 as the final reaction product. Due to such mechanism the reaction proceeds through two current peaks in the positive scan. At low potentials the current increases as a result of dehydrogenation, i.e. the direct path, based on the oxidation of formate [7] as the active intermediate, which does not need any oxygen-containing species [8] to be oxidized to CO_2. Simultaneously CO_{ads} is generated through dehydration in parallel path, reducing the number of Pt sites available for the direct path, and as a result the current slowly rises until it reaches a plateau. Subsequent formation of oxygen-containing species on Pt enables the oxidative removal of CO_{ads}. This allows more Pt sites to become available for HCOOH oxidation and current increases again until the formation of Pt oxide, inactive for HCOOH oxidation, begins. In the reverse scan the reaction proceeds through a single peak. Oxidation of formic acid, as the oxidation of adsorbed CO, strongly depends on crystallographic orientation of the Pt surface [9]. The reaction is almost inhibited at Pt(100) and Pt(110) single crystals and only at high potentials, with the formation of PtOH when the poisoning species are oxidized, the current starts to increase. In the case of Pt(100) surface only a small peak appears at 0.8 V versus RHE (Reversible Hydrogen Electrode), while at Pt(110) the increase in current is significant and located at a more negative potential (0.68 V versus RHE). On the other hand, at Pt(111) formic acid is oxidized through a bell shaped single peak positioned at 0.6 V versus RHE, but with rather low currents. Although the least poisoned, this surface still exhibits low activity. In the reverse scan at Pt(111) the sweep retraces the forward one, at Pt(110) there is a sudden, sharp rise of current, reaching a maximum at about 0.7 V, while at Pt(100) the increase in current is not so sharp and the peak is reached at 0.4 V. Pt(100) is the most active electrode, followed by Pt(110) whereas the least active one is again Pt(111) [10].

Having this structural sensitivity in mind, not only for these two reactions but for some other ones as well, synthesis of nanoparticles with desired crystal habit is lately becoming a focus of research. Usually, in those syntheses, besides a Pt precursor and reducing agent, an organic compound is present to prevent particles from agglomeration, and in order to control the particle shape some capping agent is added as well [11,12]. The role of these agents is to stabilize the specific crystal facet through chemical interaction that alters its free energy and slows down its growth rate. This results in the desired facet prevailing on the surface of the formed particle. A variety of synthesis procedures has been developed [11–13], one of which is the water-in-oil (W/O) microemulsion method. This method implies the implementation of the reduction reaction inside the microreactors that consist of reverse micelles. Microemulsions are formed by the dispersion of a water phase in a nonpolar, oil phase, with a surfactant as phase boundary. The water phase consists of a precursor solution with the possible addition of a capping agent. As the water phase is trapped inside the reverse micelles, where all processes take place, this system can be regarded as a group of microreactors inside the oil phase. If the water phase consists only of the water solution of the precursor, particles synthesized with W/O microemulsion method have cube-octahedron shape (quasi sphere), with the size of 3–7 nm [14]. If a proper amount of HCl, as the capping agent, is added to the water phase, it is possible to form particles with cubic shape and with particle size of 12–14 nm [14].

The aim of the present study was to synthesize shape controlled Pt nanoparticles with the smaller size than reported in the literature. We modified the microemulsion method proposed by Martinez-Rodrigez et al. [14] by using the reducing agent in a large excess and introducing high area carbon into the microemulsion. The structural analysis of the Pt/C powder prepared in this way revealed that Pt particles were 2–6 nm in diameter with the significant proportion of concave cube shaped ones when optimum amount of HCl as capping agent was applied. The presence of high area carbon support enabled complete removal of organic residues from Pt nanoparticles after the synthesis. Accordingly, the electrochemical cleaning treatment that could induce reconstruction of the Pt surface was avoided. The electrochemical characterization demonstrated the presence of preferentially oriented facets at the

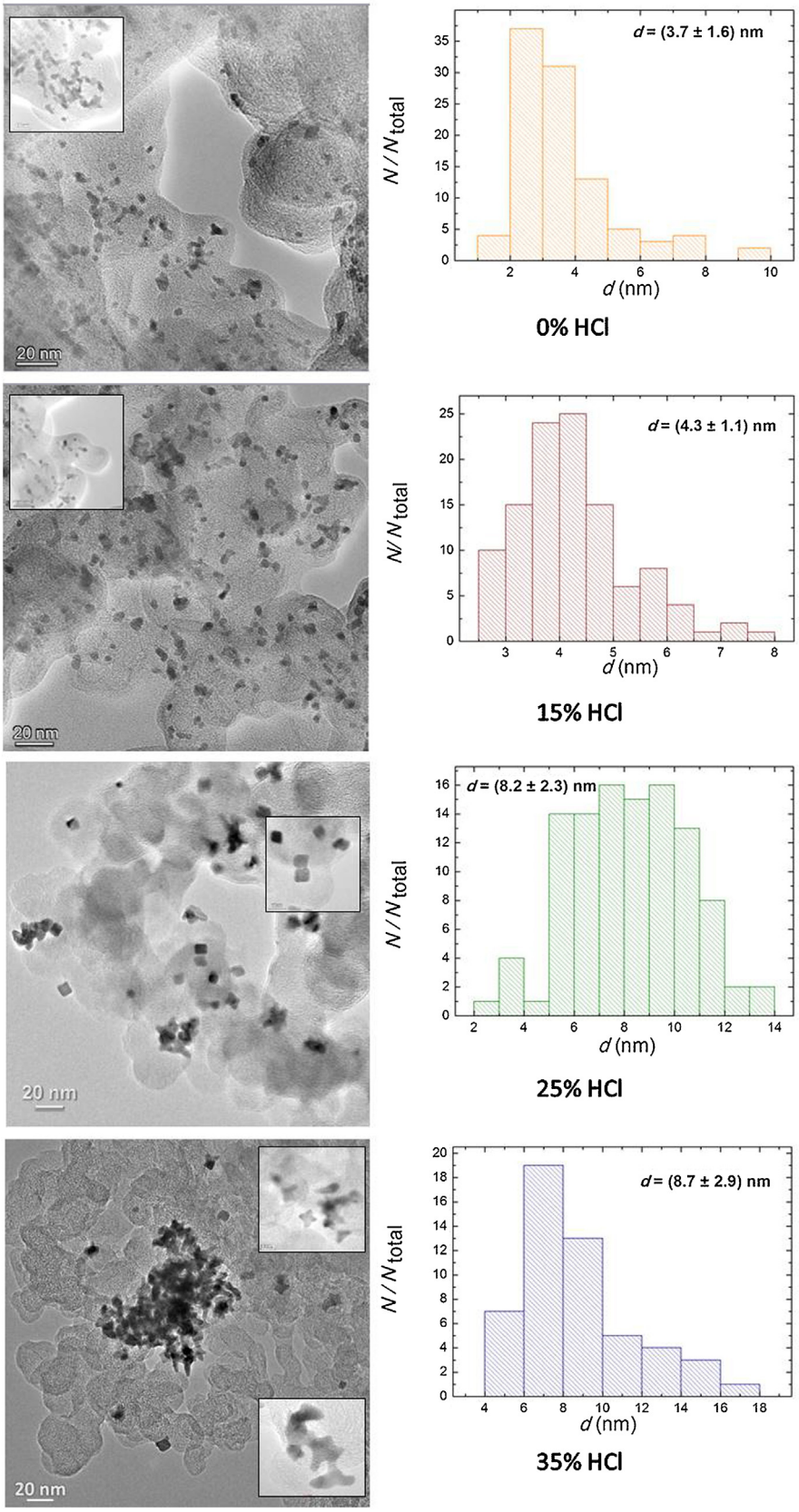

Fig. 2. TEM images and particle size distributions of supported Pt/C catalysts. Images with higher resolution are reproduced in the insets.

shaped particles and their increased activity for the formic acid oxidation.

2. Experimental procedures

2.1. Preparation of the catalysts

Catalysts were synthesized using water-in-oil microemulsion method. Precursor H_2PtCl_6 present in the water phase of this system {water|polyethyleneglycol-dodecylether (BRIJ®30)|*n*-heptane}, was reduced by $NaBH_4$. BRIJ®30 was used as a surfactant, while different amounts of HCl as capping agent were incorporated in the water phase (0, 15, 25 and 35%), in order to produce Pt nanoparticles with different shape and structural characteristics. Water to surfactant molar ratio was $\omega_0 = 3.8$, while the amount of surfactant, in volume, equalled to 16.5% of the total volume of the microemulsion. The concentration of the precursor present in the water phase was 0.1 M H_2PtCl_6. The amount of reducing agent was in a large excess, with the $NaBH_4$ to Pt molar ratio of 50: 1. Formed Pt nanoparticles were supported on Vulcan XC-72R after the completion of the reduction reaction. Vulcan XC-72R was added as a powder in the microemulsion, and the mixture was stirred for 5 h in order to load Pt nanoparticles on the support. Nominal content of Pt in catalyst powders was 20 wt%. Acetone was added in the final step in order to destabilize the microemulsion and cause precipitation. After complete phase separation that took place overnight the precipitate was later washed thoroughly with ultra-pure water (Millipore, 18 MΩ) on a membrane filter, using vacuum pump, and dried in N_2 atmosphere at 170 °C for 3 h. It should be noted that it would not be possible to wash unsupported Pt nanoparticles on any filter because of their small size.

2.2. Characterization of the catalysts

XRD experiments were performed on an X-Pert powder diffractometer (PANalytical, Netherlands) using CuKα radiation in Bragg-Brentano geometry at 40 kV and 30 mA. The measurements were conducted in a step scan mode in 0.05° (2θ) intervals with a measuring time of 30 s/step. The TOPAS V3 general profile and structure analysis software for powder diffraction data was used for the Rietveld refinement procedure [15].

The supported catalysts were investigated on a FEI TITAN^3 Themis 60–300 double aberration corrected TEM. Samples were drop cast onto Holey carbon grids and investigated at 200 kV operating voltage by CTEM (conventional transmission electron microscopy) and STEM (scanning transmission electron microscopy). Investigations were performed at the Center for Nanoanalysis and Electron Microscopy (CENEM), University of Erlangen. The mean particle size and size distribution were acquired from a few randomly chosen areas of each sample by taking 100 particles into account.

2.3. Electrochemical measurements

All of the electrochemical experiments were performed at room temperature in three-electrode-compartment electrochemical cell with a Pt wire as the counter electrode and a bridged saturated calomel electrode (SCE) as the reference electrode. All potential values presented in this paper are given versus SCE. The working electrode was a thin layer of Nafion-impregnated Pt/C catalyst applied on a polished glassy carbon disk electrode with the Pt loading of 20 μg/cm^2. The thin layer was obtained from the suspension of the respective catalyst in a mixture of 1 ml water and 50 μl of 5% aqueous Nafion solution. After dispersion in an ultrasonic bath, 10 μl of the suspension were placed on the electrode and dried at room temperature.

The electrocatalytic activities of Pt/C catalysts were studied in 0.5 M H_2SO_4 + 0.5 M HCOOH solution. HCOOH was added to the supporting electrolyte solution while holding the electrode potential at – 0.2 V. The potential was then cycled up to 0.9 V at sweep rate of 50 mV/s. Long-term stability of the catalysts was tested for formic acid oxidation (FAO) during 100 cycles in this potential range and by chronoamperometric measurements. Current-time transient curves were recorded after immersion of the freshly prepared electrode in the solution at 0.2 V and holding the electrode at that potential for 30 min.

The real surface area was determined from the CO stripping voltammetry. CO was adsorbed at the electrode surface from CO saturated 0.5 M H_2SO_4 solution while keeping the electrode potential at – 0.2 V for 15 min. Subsequently, the electrode was transferred into the cell containing only 0.5 M H_2SO_4 and the adsorbed CO was electrochemically oxidized at a sweep rate of 50 mV/s. Three subsequent voltammograms were recorded to verify that CO has been completely removed. The real surface area was estimated by the calculation of the charge from CO_{ads} stripping voltammograms corrected for background currents (assuming 420 μC/cm^2 for the CO monolayer). The oxidation of CO_{ads} and formic acid was studied at separate surfaces, which featured similar basic voltammograms.

Oxidation of ammonia (0.3 M) in 0.1 M NaOH at a sweep rate of 50 mV/s was used as a probe for {100} planes.

All the solutions were prepared from Merck p.a. reagents with high purity water (Millipore, 18 MΩ/cm resistivity). The electrolytes were purged with purified nitrogen prior to each experiment. AUTOLAB potentiostat/galvanostat PGStat 128 N (MetrohmAutolab B.V., The Netherlands) was used in electrochemical experiments.

3. Results and discussion

3.1. Physicochemical characterization of the catalysts

The aim of this research was to prepare carbon supported Pt catalysts with particles small in size and with various shapes. For this purpose we used the water-in-oil microemulsion synthesis with and without the addition of HCl, similarly as described by Martinez-Rodriguez et al. for unsupported catalysts [14], but with large excess of reducing agent.

At a glance, XRD analysis of the prepared catalysts shown in Fig. 1 revealed the distinctions between the catalysts prepared with higher HCl amount. All diffraction patterns exhibit a diffraction peak at around 25° (2θ) related to a graphite-like structure of the Vulcan support and the characteristic diffraction peaks of the *fcc* platinum crystalline structure ([03-065-2868] ICDD-PDF). Rietveld analyses of these patterns, presented in Table 1, confirmed that the particles with smaller crystallite size were formed, being below 4 nm when no HCl or only 15% of the acid was used and below 8 nm if higher quantity up to 35% of the acid was added. Pt lattice constant also decreased with the addition of HCl indicating changes in the interplanar spacing d_{hkl}. Relative contributions of individual crystallographic planes indicated the highest fraction of {110}. According to the accepted model, nanoparticles are of cubooctaedron (quasi spherical) shape with preferential {100} and {111} facets, while {110} atomic positions are associated with corners and edges [16,17]. Having this in mind, the decrease in the share of {110} plane with the addition of HCl accompanied with the increase in the crystallite size, might indicate the modification in the crystal habit.

The changes in the particles shape were verified by TEM characterization. The images recorded for all four catalysts (Fig. 2) disclose their differences and show the agglomeration of the particles. The

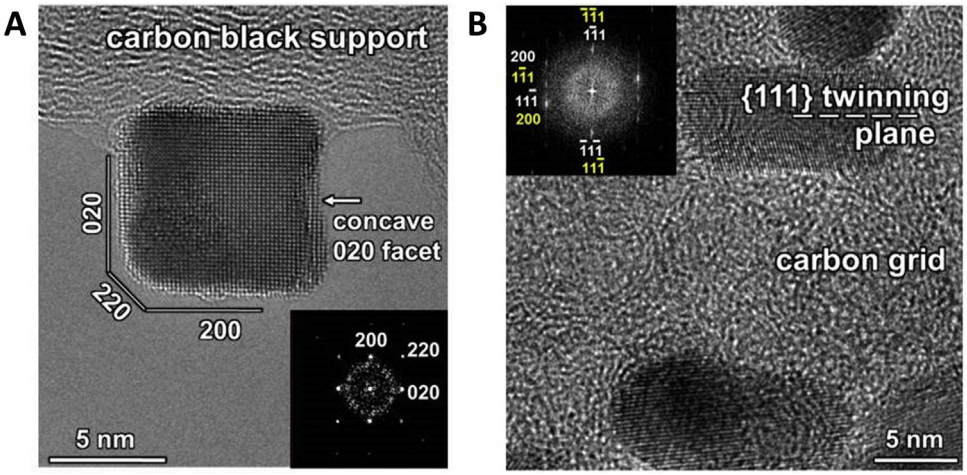

Fig. 3. High resolution TEM images of concave cubic (A) and twinned (B) Pt particles synthesized with 25% HCl. Corresponding FFT patterns of Pt particles are presented in the insets.

Table 1
Structural parameters obtained from XRD analysis of Pt/C catalysts.

Sample designation	Crystalline phase	Crystallite Size (nm)	Lattice Constant (Å)	Relative contributions of Pt crystallographic planes (%)		
				(111)	(200)	(220)
Pt/C – 0% HCl	Pt	2 ± 1	3.928	12	25	63
Pt/C – 15% HCl	Pt	3 ± 1	3.913	14	25	61
Pt/C – 25% HCl	Pt	4 ± 1	3.910	20	23	57
Pt/C – 35% HCl	Pt	6 ± 1	3.910	26	23	51

mean crystallite size is in good accordance with the XRD results, within the evaluation error. Catalysts with 0% or 15% of HCl used are 4 ± 2 nm in size while the catalysts prepared with 25 and 35% of HCl have particles of 8 ± 3 nm. Based on the images recorded in higher resolution, the addition of small amount of HCl (15%) did not induce any change of the particle shape (quasi spherical particles are formed), while increased acid quantities led to the formation of cubes for 25% HCl or various shapes (truncated cubic, but also branched-like structures [18]) for 35% HCl (insets in Fig. 2). However, in the last two samples spherical particles were also present and it can be estimated that about 50% of the particles attained specific shapes. Yet, the synthesis performed with 25% HCl produced particles with a much more cuboidal shape than synthesis with 35% acid, which can be seen from low magnification – high resolution images such as Fig. 2C and D. We suppose that the incomplete transformation to cuboidal particles is probably due to the unbalanced ratio between the quantity of the capping and reducing agents.

As previously mentioned, changes in the crystal habit are induced when free energy of a certain crystal facet is changed due to the chemical interaction with a capping agent which slows its growth rate [12]. For isolated, un-twinned crystals the direction of the fastest growth is parallel to the largest diameter of the crystal. Therefore, it is to expect that in our case the crystal habit is determined by the relative growth rates of {100} and {111} crystallographic planes. This is supported by the growth parameter α (Eq. (1)), where V_{100} and V_{111} are the growth rates of these facets.

$$\alpha_{3d} = \sqrt{3}\frac{V_{100}}{V_{111}} \quad (1)$$

For $\alpha \leq 1$, idiomorphous crystals grow in the form of cubes, for $1 < \alpha < 3$ in the form of cubo-octahedra and for $\alpha \geq 3$ in the octahedral form [19]. Since the catalyst prepared with 25% HCl has cubic-shaped particles, we can presume that $\alpha = 1$ i.e. that the growth rate of the {111} facet is higher or similar to the {100} facet.

The catalysts prepared with the addition of 25% or 35% HCl were analyzed by high resolution TEM (HRTEM). HRTEM for the catalyst synthesized with 25% HCl reveals that particles are actually concave cubes. We assume that the reason for this concavity is the introduction of large excess of the reducing agent. This probably led to the higher reduction rate in comparison to the surface diffusion rate, so that reduced Pt atoms rather nucleate and grow from the edges and corners than migrate to the surface [20]. A particle presented in Fig. 3A has facets with {020}, {220} and {200} orientation. Facets are flat surfaces, while the concave shape comes from small steps and kinks present on those facets. Fast Fourier Transform (FFT) pattern confirms this shape. Beside single cubic, twinned particles were also observed (Fig. 3B). The presented particle has twin occurring with the {111} twinning plane stretching across the middle of the particle. In FFT pattern (inset in Fig. 3B) Miller indices in yellow represent twins above the twinning plane, while in white represent twins below the twinning plane. Twinning plane (twin boundary) separates two parts of Pt crystal which share some of the same lattice points in a symmetrical manner (twinning plane is in fact a mirror plane). HRTEM images of the particles synthesized with 35% HCl are shown in Fig. 4. The particle in Fig. 4A consists of {111} planes, with facets being of {110} orientation. Although it is slightly tilted around [100] direction and it is off [100] zone axis, this image still shows cuboidal shape, {200} plane lattice fringes, and concave {200} facets. Agglomerated particles are displayed in Fig. 4B. Facets with {200} and {111} orientation are present.

Martinez-Rodriguez et al. [14] obtained, with the addition of 30–37% HCl, "bone-like" particles ascribing the phenomena to HCl etching. On the other hand, Ma et al. [21] reported preparation of branched Pt nanocrystals by HCl oxidative etching and tailoring the number of branches by varying the acid concentration. According to these authors, HCl can influence atomic addition onto single-crystal seeds. Atomic addition is associated with the surface facets on which atoms should be added, as well as with the kinetics of

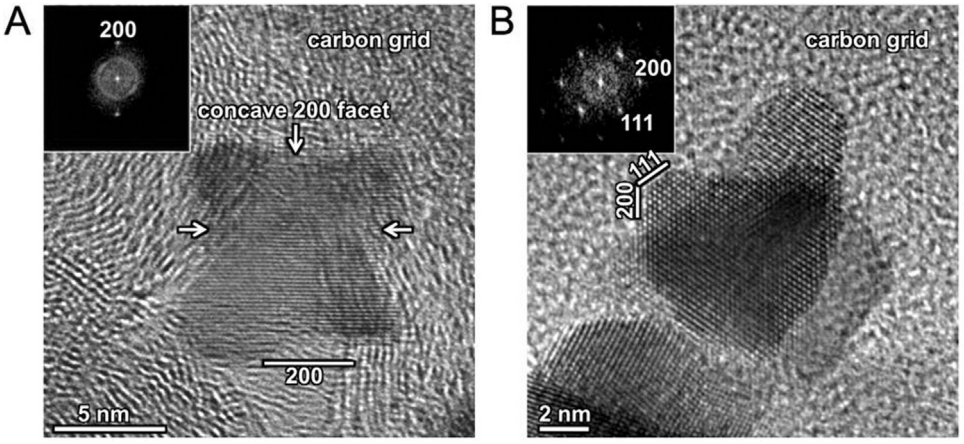

Fig. 4. High resolution TEM images of cuboidal (A) and agglomerated (B) Pt particles synthesized with 35% HCl. Corresponding FFT patterns of Pt particles are presented as insets; concave 200 facets in A (left image) are indicated by white arrows.

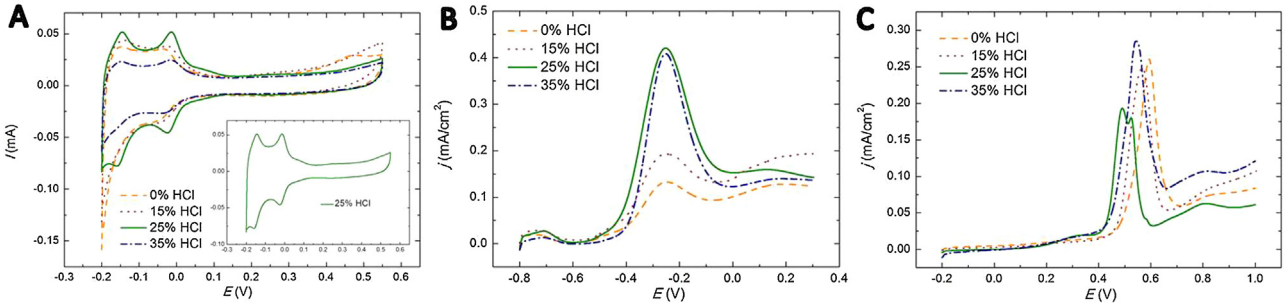

Fig. 5. Cyclic voltammograms of as prepared Pt/C catalysts in 0.5 M H_2SO_4, v = 50 mV/s (A); amonia oxidation (0.3 M) at as prepared Pt/C catalysts in 0.1 M NaOH, v = 50 mV/s (B); CO_{ads} stripping curves for as prepared Pt/C catalysts in 0.5 M H_2SO_4, v = 50 mV/s (C).

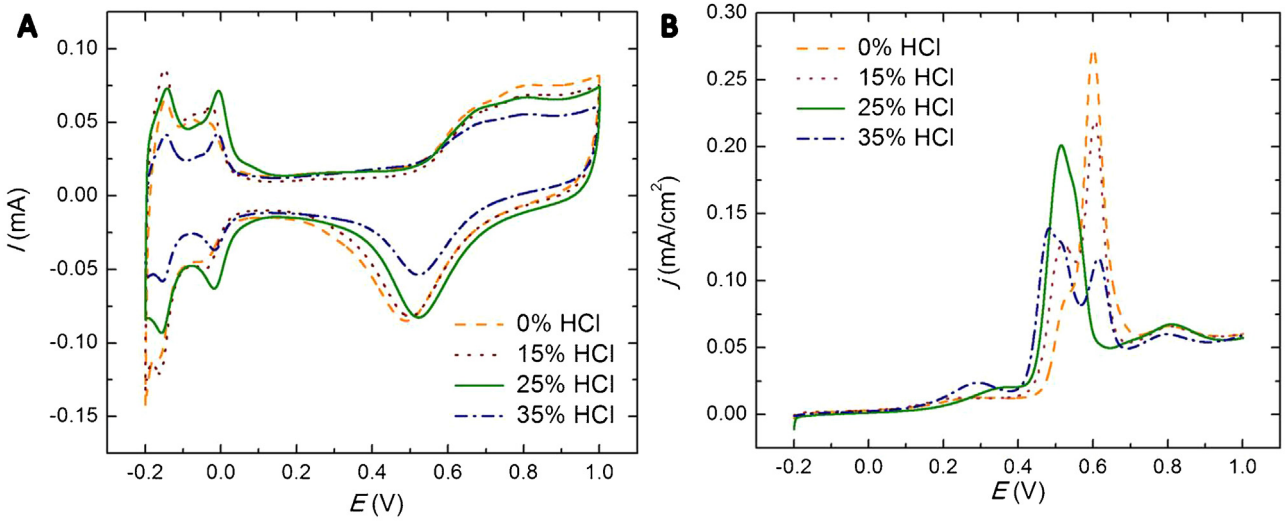

Fig. 6. Cyclic voltammograms of ox.-annealed Pt/C catalysts in 0.5 M H_2SO_4, v = 50 mV/s (A); CO_{ads} stripping curves for ox.-annealed Pt/C in 0.5 M H_2SO_4, v = 50 mV/s (B).

atomic supply. Increasing acidity in synthesis in air (thus O_2/Cl pair in the case of HCl) can induce strong oxidative etching which can markedly retard the generation of freshly formed atoms. This in turn would slow down the rate of atomic addition resulting in the formation of highly branched particles from cuboctahedral seeds [21–23]. The etching process occurs on sites with high reactivity such as defects, corners and edges as well as twinned planes [18]. Having this in mind, it can be speculated that variously shaped particles and branched-like structures of our catalyst synthesized with the addition of 35% HCl might occur due to the etching properties of HCl.

3.2. Electrochemical characterization of the catalysts

All the Pt/C catalysts were also characterized by cyclic voltammetry. An initial scan of each *as prepared* catalyst, thus without any electrochemical treatment, is presented in Fig. 5A.

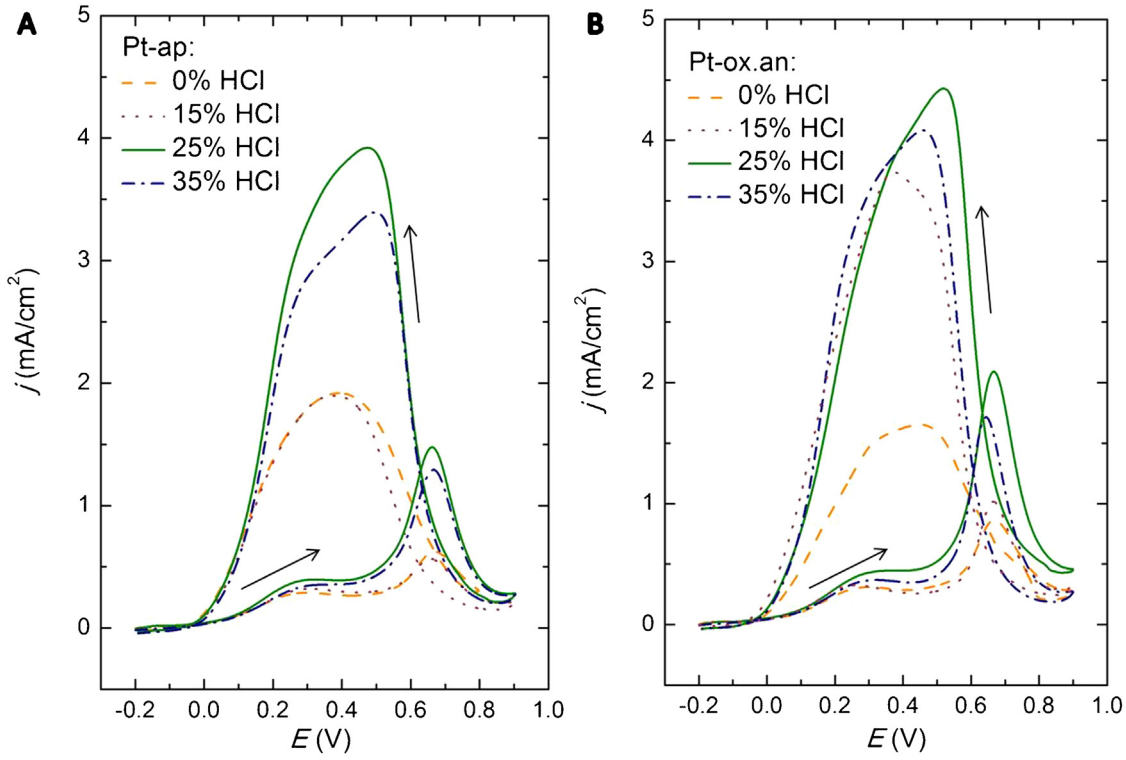

Fig. 7. Potentiodynamic curves for the oxidation of 0.5 M HCOOH at as prepared (A) and ox.-annealed (B) Pt/C catalysts in 0.5 M H_2SO_4, v = 50 mV/s.

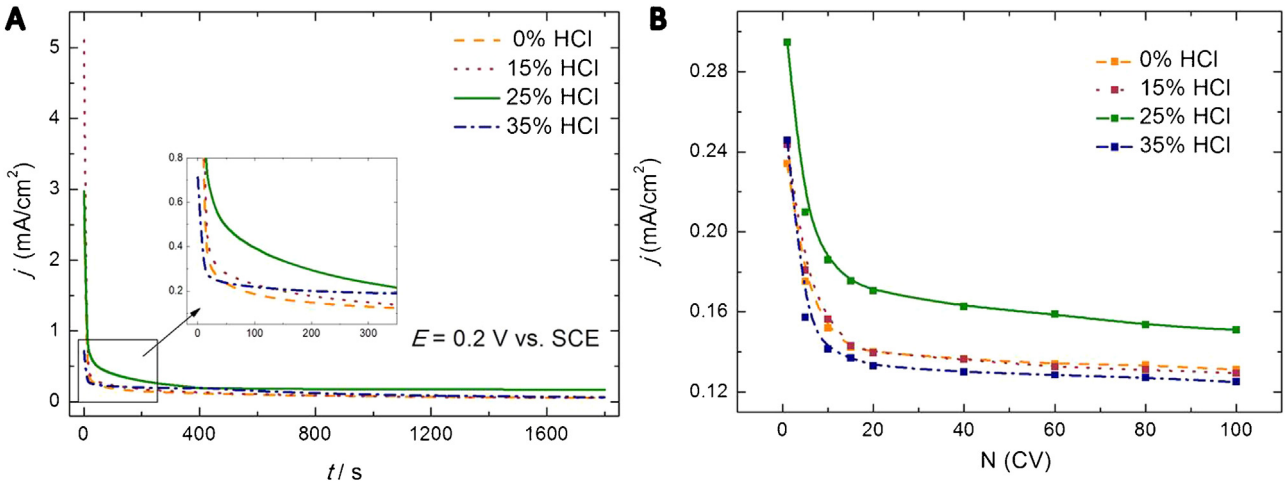

Fig. 8. Chronoamperometric curves for the oxidation of 0.5 M HCOOH in 0.5 M H_2SO_4 at as prepared Pt/C catalysts at 0.2 V (A); long-term stability of as prepared Pt/C catalysts versus the number of scans during formic acid oxidation (current values taken at 0.2 V; v = 50 mV/s).

It is noteworthy that all *as prepared* catalysts exhibit characteristic peaks that are fingerprints of the H_{UPD} on {110} atomic positions and atomically ordered sites on {100} surfaces [16,24,25]. These peaks are defined despite the absence of any additional electrochemical cleaning treatment [26]. This means that quite clean particles are prepared, probably due to thorough washing and the mild thermal treatment of the supported particles at the end of the synthesis process, when the residual surfactant, if any, has been removed [27]. However, only for the catalyst synthesized with 25% HCl, the one featuring concave cubic particles, these peaks are well pronounced and even more a shoulder at 0.08 V versus SCE is recorded, as well as a small broad peak at 0.25 V (inset in Fig. 5A). A similar voltammetric profile was registered by Urchaga et al. [25] and by Martinez-Rodriguez et al. [14] for electrochemically cleaned unsupported quasi-spherical particles prepared by water-in-oil microemulsion synthesis with borohydride as a reducing agent, and no capping agent. Significantly pronounced features were recorded for unsupported electrochemically cleaned Pt particles in exclusively cubic shape [14,25]. According to the authors, these features should correspond to atomically ordered short and long range {100} terraces and anion adsorption/desorption on {111} surfaces respectively, with the intensities depending on the fraction of the domains on the surface. Since our catalysts have only a portion of preferentially ordered nanoparticles, these additional characteristics have rather low intensity.

Studies of ammonia oxidation in alkaline solution at low index Pt single crystals [28] and on large number of different stepped surfaces [29] have demonstrated that this reaction proceeds almost

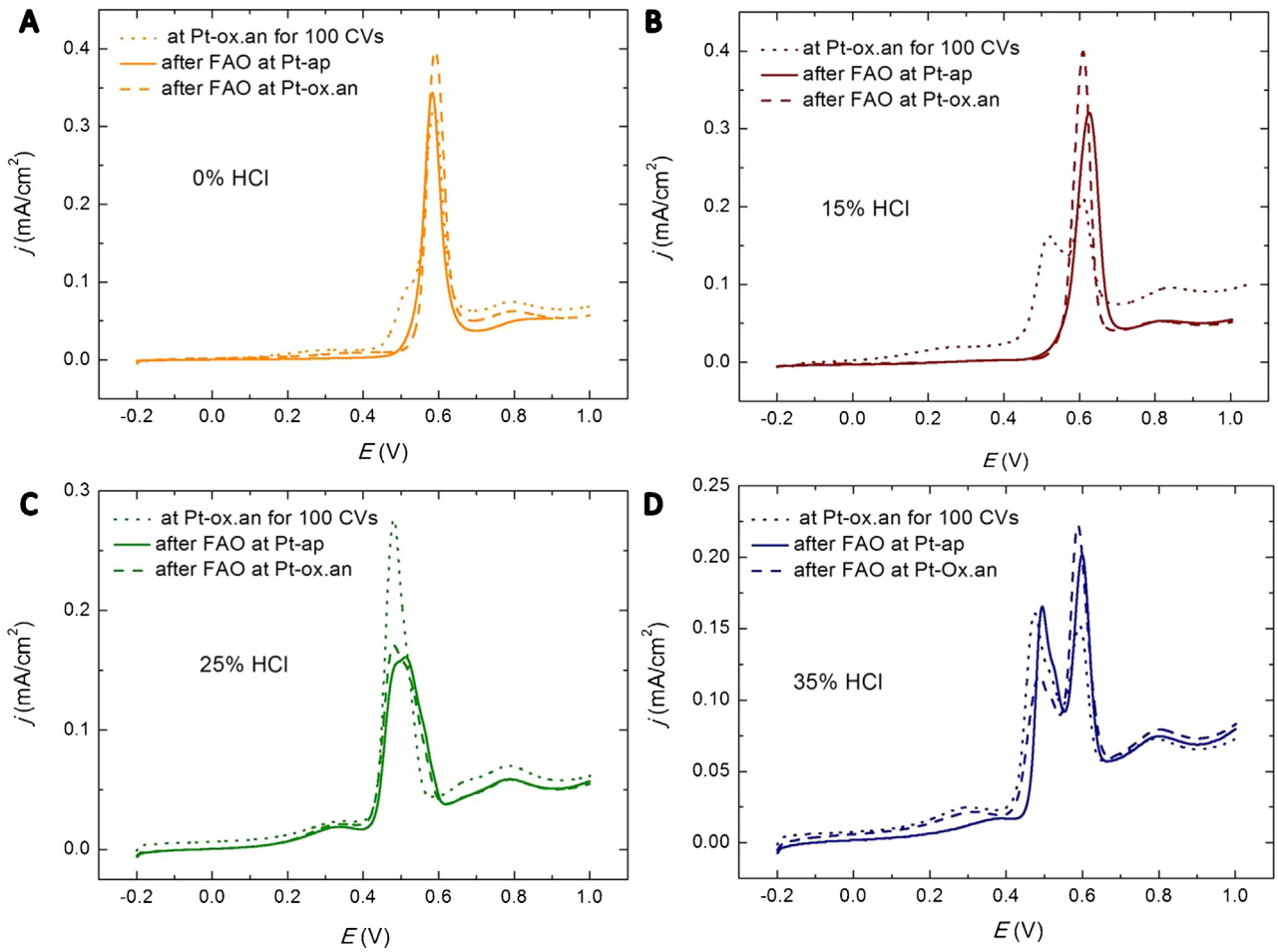

Fig. 9. CO_{ads} stripping curves for as prepared and ox.-annealed Pt/C catalysts in 0.5 M H_2SO_4, v = 50 mV/s after 100 cycles without and with 0.5 M HCOOH.

only on Pt{100} surfaces. The activity of the electrode is determined by the width of {100} terraces. However, short {100} terraces containing {111} steps exhibit higher current densities than {100} terraces having {110} steps although oxidation of ammonia is strongly inhibited on both {111} and {110} surfaces [29]. This dependence was corroborated by the oxidation of ammonia on differently shaped nanoparticles prepared by water-in-oil microemulsion with HCl as capping agent, when cubic particles exhibited highest activity [14]. We used this reaction to verify the presence of wide {100} facetes on our catalysts prepared with the addition of HCl. The results are shown in Fig. 5B and, as can be seen, catalysts with concave-cubic and branched-like particles manifest noticeably higher activity in comparison to quasi spherical ones. Although branched-like particles should not have wide {100} planes they are as active as concave-cubic particles probably because they are in junction with {111} atomic planes (Fig. 4B), which is also favorable for the oxidation of ammonia [29].

Being extremely sensitive to surface structure, oxidation of CO_{ads} was applied for the characterisation of the Pt/catalysts as well as for the determination of their electrochemically active surface area. Stripping curves for CO_{ads} on the *as prepared* Pt/C are presented in Fig. 5C. The catalysts synthesized with larger amount of HCl are distinguished from the other two catalysts. While for the quasi spherical particles oxidation of CO_{ads} proceeds at more positive potentials (peak at ~0.6 V, the onset potential at 0.45 V) due to their significantly smaller size, for shaped particles the reaction is shifted to lower potentials and a pre-peak is recorded. This pre-peak could be described as the oxidation of CO that is weakly adsorbed due to CO—CO repulsive interaction, which are characteristic for {100} and {111} planes [5,30] containing surface defects [25]. Although the onset potential is the same for both catalysts, the one where branched-like particles prevail exhibits a single oxidation peak, whilst for concave-cubic particles the splitting of the CO_{ads} oxidation peak is observed. This peak multiplicity is related to the surface structure and here is the consequence of concave-cubic particle shape. The CO_{ads} stripping profile and peak potentials are in accordance with those presented in literature for preferentially oriented particles [25,30,31] where it has been demonstrated that the intensity of the peak at a higher potential increases with the increase of a fraction of {100} plane. Therefore, the peak at a higher potential should reflect the oxidation from the {100} facetes while the peak at a lower potential could be the contribution from the oxidation of CO_{ads} from {111} preferentially oriented planes [25,30]. However, since the particles are concave cubic with concavity coming from small steps and kinks present on the flat facets (Fig. 3), this peak at lower potential should be primary associated with CO_{ads} oxidation due to OH formed on these sites [3,4].

As already mentioned, we synthesized carbon supported Pt/C catalysts according to the procedure described in literature for unsupported catalysts [14]. In order to clean the unsupported particles, the authors used a two-step protocol that included washing the particles with acetone and ultrapure water followed by the cycling the potential between −0.2 and 1.0 V until a stable voltammogram was attained [32]. For that reason we also subjected our catalysts to the electrochemical treatment comprising 20 cycles

in the supporting electrolyte and designated it as oxide (ox.-) annealed.

Steady state voltammograms of ox.-annealed Pt/C catalysts are displayed in Fig. 6A. These voltammetric profiles reveal pronounced characteristic peaks for {110} atomic plane and {100} steps and terrace borders in the hydrogen adsorption/desorption region separated from well-defined oxide formation/reduction region by a double layer area. It should also be mentioned that, although more weakly defined, the features assigned to {100} terraces or wide facets and {111} atomic planes are still recorded on the CV for Pt/C catalyst containing concave-cubic particles (25% HCl). It seems that the catalyst surfaces have been reconstructed and cleaned from impurities. However, the electrochemically active surface area (ECSA) calculated from CO_{ads} stripping voltammetry for these ox.-annealed surfaces, in comparison to the one calculated for *as prepared* catalysts, decreased only by $15 \pm 3\%$ retaining the same order. Namely, the highest values were reckoned for quasi spherical (smaller) particles, than for the catalysts having a portion of concave-cubic particles, and the lowest value was obtained for the catalyst with branched-like structures, probably because of their significant agglomeration. Cycling the potential to 1.0 V or higher can induce particle migration and coalescence [33–35], as well as Pt dissolution [36,37], which causes the decrease in ECSA. The decrease of ~15% after ox.-annealing of our catalysts is much smaller compared to other catalysts treated similarly [38], which supports the assumption that Pt particles synthesized by the modified water-in-oil procedure have clean but also rather stable surfaces.

Oxidation of adsorbed CO used for ECSA calculation, revealed the surface morphology of ox.-annealed catalysts (Fig. 6B) as well. At the ox.-annealed Pt/C with quasi-spherical particles (0% and 15% HCl), the CO_{ads} oxidation commences practically at the same potentials as at the *as prepared* surfaces. The peak is shifted for some 20 mV to higher values, but an additional shoulder (peak) at the onset of the reaction appears in the stripping voltammograms (Fig. 6B). These two features indicate two settlements of CO and two types of OH species [39,40]. The coalescence of the particles into agglomerates, induced by potential cycling during ox.-annealing, produces a high density of defects, such as steps and grain boundaries on the borders of coalesced particles [39]. These formations are generally considered to be more active than terraces for the oxidation of CO [41–44]. Smaller single particles have fewer numbers of defects and higher CO and oxygen binding energy, due to the electronic structure induced by size constraint [39]. Therefore, the shoulder (peak) at lower potential should be assigned to CO_{ads} oxidation at agglomerated particles and the one at higher potential to the reaction at single particles. In the case of the catalysts containing concave-cubic particles (25% HCl), the pre-peak region and the onset potential remain practically unchanged as at the *as prepared* one, but the profile of the main peak at ox.-annealed surface is changed. Instead of multiplied, it is now asymmetric due to the decrease of wider {100} facetes upon potential cycling. Contrary to this catalyst, the oxidation of CO_{ads} at the ox.-annealed Pt/C prepared with the highest quantity of HCl (35%) proceeds through a pre-peak shifted to a bit lower potentials, followed by two peaks separated by 130 mV. Moreover, careful analysis disclosed that the first peak, after the current maximum at 0.48 V, also includes a shoulder at 0.51 V, that coincides with the potentials reflecting oxidation of CO_{ads} from {111} preferentially oriented atomic planes and {100} facetes, respectively, as proposed in the literature [25,30]. We suppose that the first asymmetric peak arises from the CO_{ads} oxidation at agglomerated and highly branched-like particles, while the second peak at a higher potential pertains to the reaction at well separated single quasi spherical particles.

3.3. Formic acid oxidation

Formic acid oxidation (FAO) was examined at both *as prepared* and ox.-annealed Pt/C catalysts. The initial scans are presented in Fig. 7.

According to the shape of the polarization curves in the forward direction, the reaction proceeds through dual path mechanism at all the catalysts. Comparing their activities, it is seen that the catalysts containing concave-cubic (25% HCl) and branched-like particles (35% HCl), exhibit higher activity than the other two catalysts in both forward and backward scans, either *as prepared* or ox.-annealed. Large hysteresis between forward and reverse scans is characteristic for Pt(100) and Pt(110) single crystals and the latter one also exhibits increased currents at higher potentials in the forward scan [9]. The voltammetric profiles of Pt/C catalysts prepared with 25% and 35% HCl are similar to the profile of quasi spherical polyoriented unsupported Pt particles prepared by the W/O method, but without addition of HCl, as reported by Solla-Gullon et al. [45]. However, the catalyst prepared with 25% HCl is twice as active in comparison to polyoriented unsupported Pt particles [45] (maximum currents in low potential region: 0.4 mA/cm^2 versus 0.18 mA/cm^2) despite the significantly larger particle size (8.2 ± 2.3 versus 4.5 ± 0.8). Namely, Park et al. [46] in their study of the particle size effect on FAO revealed considerably higher reaction rate on the particles with a diameter below 4 nm than on the larger ones. It is worth noting that even our catalysts with quasi spherical particles (0% and 15% HCl), with sizes similar to those described by Solla-Gullon et al. [45], exhibit increased activity (maximum currents in low potential region: 0.3 mA/cm^2 versus 0.18 mA/cm^2). More importantly, the catalyst with concave-cubic particles (25% HCl) is more active in comparison to unsupported catalyst with cubic particles described by the same authors [45] (maximum currents in low potential region: 0.4 mA/cm^2 versus 0.28 mA/cm^2). Being of similar particle size, these differences in the activity and FAO profile should be related to their surface structures. Obviously, steps and kinks present on the concave facets of Pt/C (25% HCl) improve the catalyst activity, as does the introduction of steps on a low index Pt single crystals [47].

Another important finding from the examinations of FAO at *as prepared* and ox.-annealed Pt/C catalysts is the almost negligible difference in the activity of these surfaces for each catalyst (Fig. 7). This result supports our assumption that carbon supported Pt catalysts prepared by modified water-in-oil microemulsion method have rather clean particles without strongly bonded impurities and with quite stable surface structure.

3.4. Stability of the catalysts

Stability of Pt/C catalysts during the oxidation of formic acid was examined by chronoamperometry and through prolonged cycling (100 cycles) in the whole potential region (Fig. 8).

Current density recorded during 1800s at constant potential of 0.2 V on Pt/C containing concave-cubic particles (25% HCl) is higher than on other three catalysts (Fig. 8A). While at less active catalysts current decays rapidly reaching low steady state values in a few minutes, at concave-cubic Pt/C current decreases slowly and stabilizes at a higher value. The decline in the current during 100 cycles of FAO at 0.2 V on Pt/C catalysts is shown in Fig. 8B. As expected, the activity continuously decreases down to $55\% \pm 3\%$ of the initial value. At the same time the ratio between the currents at low potentials (first peak) and currents at high potentials (second peak) also decreases (not shown). This means that as the number of cycles increases, participation of a direct path mitigates, while the role of an indirect path in the reaction increases. However, concave-cubic catalyst remains more active during the whole test. In addition, as in the chronoamperometric measurements,

current density decreases slowly in comparison to other catalysts during long-term cycling. The decrease in the activity of Pt/C catalysts could be due to gradual accumulation of reaction residues i.e. poisoning of the electrode surface. It could also be due to the structural changes of the platinum nanoparticles, as a consequence of the potential cycling, especially in the presence of the adsorbing species (HCOOH and CO).

The characterization of the *as prepared* and ox.-annealed Pt/C surfaces after the long term potential cycling in the presence of HCOOH was performed by the oxidation of adsorbed CO. For comparison, the catalysts were also subjected to the potential cycling in the supporting electrolyte without HCOOH and then probed by CO oxidation. The results are presented in Fig. 9.

If one compares the results for each of the Pt/C catalysts, the as prepared and ox.-annealed Pt/C surfaces exposed to 100 cycles of FAO give similar CO_{ads} oxidation profiles. However, significant difference between the catalysts of different particle shape is observed. On the quasi-spherical particles the oxidation of CO_{ads} proceeds through one symmetric sharp peak, similarly to the one for *as prepared* surface prior to FAO (Fig. 5C), but positively shifted for about 0.07 V. Since the oxidation of CO commences at higher potentials on the smaller particles [48], this is an indication of a decrease in particle size during the potential cycling in the presence of HCOOH [38]. On the other hand, Pt/C catalysts containing concave-cubic and branched-like particles, exhibit completely opposite properties upon similar treatment. CO_{ads} stripping profiles for these catalysts are similar to the ones for ox.-annealed surfaces prior to potential cycling in HCOOH containing electrolyte (Fig. 6B).

When the catalysts are subjected to potential cycling (100 cycles) in the absence of HCOOH (Fig. 9), the oxidation of CO_{ads} follows the similar pattern as at ox.-annealed surfaces (Fig. 6B), with negligible difference in the potential values for each catalyst. This means that marked changes in the surface morphology occur during first 20 cycles when steady state is achieved. The additional decrease of ECSA of ~6% during this long-term cycling in comparison to the values for ox.-annealed surfaces supports this conclusion.

Considering all these results, it can be concluded that quasi-spherical particles undergo more drastic changes by cycling in the presence of HCOOH than in its absence (Fig. 9A and B). On the other hand, potential cycling in the supporting electrolyte without or with HCOOH for the Pt/C catalysts containing concave-cubic and branched-like particles triggers rather similar perturbations in the surface morphology (Fig. 9C and D). As already mentioned, cycling the potential to 1.0 V or higher can induce particle migration and coalescence [33–35] as well as Pt dissolution [36,37]. Noticeable dissolution of Pt occurs upon more severe treatment [49–51]. Considering that FAO proceeds on Pt/C through both direct – dehydrogenation and indirect – dehydration path and that during potential cycling the reaction turns more to the latter one, in which CO adsorbs on the surface, it seems that the adsorption and oxidation of CO contribute not only to particle agglomeration, but to Pt dissolution as well. Few studies were devoted to the relationship of the dissolution of Pt during FAO with the activity and durability of the catalyst, indicating the significant impact of the FAO on the Pt dissolution rate [52,53]. The steady loss of Pt during cycling in the supporting electrolyte containing formic acid has been confirmed by XPS, while SEM and AFM reveal morphological changes accompanying the Pt dissolution process [52]. Dissolution of Pt is a particle-size dependent reaction, i.e. smaller particles (diameter smaller than ~4 nm) undergo direct electrochemical oxidation to Pt^{2+} ions while an oxide is formed on larger particles [54]. Moreover, dissolution of Pt depends on its crystallographic orientation, i.e. Pt{111} facets dissolve considerably at higher potentials (1.15 V/RHE) in comparison to Pt(100) and Pt(110) which are more resistant due to the formation of an oxide layer [55]. Hence, we suppose that smaller quasi-spherical particles lose the catalytic activity predominantly due to Pt dissolution and morphological changes while the formation of oxide, inactive for FAO, prevails in the activity loss of larger particles. Accumulation of the reaction residues during FAO has its role as well. However, Pt/C catalyst containing concave-cubic particles remains more active because of its crystallographic surface structure.

4. Conclusions

Carbon supported platinum nanocatalysts with different particle structure were successfully synthesized by water-in-oil microemulsion method, with $NaBH_4$ as reducing, and HCl as capping agent. Addition of the catalyst support in the synthesis process facilitated the catalyst cleaning procedures, thus enabling the application of the prepared catalysts without any additional electrochemical treatment, in their *as prepared* state.

XRD and TEM results revealed that synthesized particles are smaller in size (4–8 nm) compared to some previously reported, which we assign to the higher amount of the reducing agent used, which enabled faster nucleation than growth of the seeds. TEM revealed the evolution of the particles shape depending on the HCl amount used in the synthesis. Low quantity of acid (15%) did not induce shape transformation and quasi-spherical particles were formed as in the absence of HCl. Formation of concave cubes was achieved with 25% of HCl. Since the reducing agent was used in large excess, reduction rate of Pt precursor was higher in comparison to the surface diffusion rate. Consequently, Pt atoms rather nucleated and grew from the edges and corners than migrated to the surface forming concave instead of regular cubes. The highest concentration of HCl (35%) used as the capping agent resulted in the synthesis of various structures which resulted from oxidative etching of sufficient HCl concentration and synthesis in air.

Particle shape evolution was documented with the voltammograms in supporting electrolyte, as well as with oxidations of CO_{ads}, ammonia and formic acid. Concave cubic particles with {100} preferential orientation showed improved catalytic properties in comparison to other catalysts, and the contribution of its preferentially oriented facets is electrochemically detectable. The results presented here clearly demonstrate that the properties of nanoparticles can be noticeably altered even by small changes in their surface structure.

Acknowledgements

This work was financially supported by the Ministry of Education, Science and Technological Development, Republic of Serbia, Contract No. 172060. V.R. Radmilovic acknowledges TEM measurement performed at the Center for Nanoanalysis and Electron Microscopy (CENEM), University of Erlangen. V.R.R. also acknowledges the support by Serbian Academy of Sciences and Arts under contract #F-141.

References

[1] S. Gilman, J. Phys. Chem. 68 (1964) 70–80.
[2] D. Strmcnik, D. Tripkovic, D. van der Vliet, K.C. Chang, V. Komanicky, H. You, G. Karapetrov, J. Greeley, V. Stamenkovic, N.M. Markovic, J. Am. Chem. Soc. 130 (2008) 15332–15339.
[3] N.P. Lebedeva, M.T.M. Koper, J.M. Feliu, R.A. van Santen, J. Phys. Chem. B 106 (2002) 12938–12947.
[4] N.P. Lebedeva, M. Koper, E. Herrero, J.M. Feliu, R.A. van Santen, J. Electroanal. Chem. 487 (2000) 37–44.
[5] N.M. Markovic, C.A. Lucas, B.N. Grgur, P.N. Ross, J. Phys. Chem. B 103 (1999) 9616–9623.
[6] A. Capon, R. Parsons, J. Electroanal. Chem. Interfacial Electrochem. 45 (1973) 205–231.
[7] A. Miki, S. Ye, M. Osawa, Chem. Commun. (2002) 1500–1501.

[8] A. Cuesta, M. Escudero, B. Lanova, H. Baltruschat, Langmuir 25 (2009) 6500–6507.
[9] A. Tripkovic, K. Popovic, R.R. Adzic, J. Chim. Phys. 88 (1991) 1635.
[10] H. Kita, H.W. Lei, J. Electroanal. Chem. 388 (1995) 167–177.
[11] Y. Xia, Y. Xiong, B. Lim, S.E. Skrabalak, Angew. Chem. Int. Ed. 48 (2009) 60–103.
[12] G.J. Leong, M.C. Schulze, M.B. strand, D. Maloney, S.L. Frisco, H.N. Dinh, B. Pivovar, R.M. Richards, Appl. Organometal. Chem. 28 (2014) 1–17.
[13] Z. Peng, H. Yang, Nano Today 4 (2009) 143–164.
[14] R.A. Martinez-Rodriguez, F.J. Vidal-Iglesias, J. Solla-Gullon, C.R. Cabrera, J.M. Feliu, J. Am. Chem. Soc. 136 (2014) 1280–1283.
[15] TOPAS V2. General Profile and Structure Analysis Software for Powder Diffraction Data, User Manual, Bruker AXS, Karlsruhe, Germany (2003).
[16] J. Solla-Gullon, P. Rodriguez, E. Herrero, A. Aldaz, J.M. Feliu, Phys. Chem. Chem. Phys. 10 (2008) 1359–1373.
[17] K. Kinoshita, in: J. Bockris, B.E. Convay, R.E. White (Eds.), Modern Aspect of Electrochemistry, vol. 14, Plenum Press, New York, 1982.
[18] R. Long, S. Zhou, B.J. Wiley, Y. Xiong, Chem. Soc. Rev. 43 (2014) 6288–6310.
[19] C. Wild, P. Koidl, W. Mueller-Sebert, H. Walcher, R. Kohl, N. Herres, R. Locher, R. Samlenski, Brenn, Diamond Relat. Mater. 2 (1993) 158–168.
[20] Y. Zhang, Q. Huang, G. Chang, Z. Zhang, T. Xia, H. Shu, Y. He, J. Power Sources 280 (2015) 422–429.
[21] L. Ma, C. Wang, M. Gong, L. Liao, R. Long, J. Wang, D. Wu, W. Zhong, M.J. Kim, Y. Chen, Y. Xie, Y. Xiong, AC Nano 6 (2012) 9797–9806.
[22] Y. Xiong, J. Chen, B. Wiley, Y. Xia, Y. Yin, Z.Y. Li, Nano Lett. 5 (2005) 1237–1242.
[23] Y. Xiong, H. Cai, B.J. Wiley, J. Wang, M. Kim, Y. Xia, J. Am. Chem. Soc. 129 (2007) 3665–3675.
[24] K. Kinoshita, J.T. Lundquist, P. Stonehart, J. Electroanal. Chem. 48 (1973) 157–166.
[25] P. Urchaga, S. Baranton, C. Coutanceau, G. Jerkiewicz, Langmuir 28 (2012) 3658–3663.
[26] J. Solla-Gullon, V. Montiel, A. Aldaz, J. Clavilier, J. Electroanal. Chem. 491 (2000) 69–77.
[27] S. Brimaud, C. Coutanceau, E. Garnier, J.-M. Leger, F. Gerard, S. Pronier, M. Leoni, J. Electroanal. Chem. 602 (2007) 226–236.
[28] F.J. Vidal-Iglesias, N. Garcıa-Araez, V. Montiel, J.M. Feliu, A. Aldaz, Electrochem. Commun. 5 (2003) 22–26].
[29] F.J. Vidal-Iglesias, J. Solla-Gullon, V. Montiel, J.M. Feliu, A. Aldaz, J. Phys. Chem. B 109 (2005) 12914–12919.
[30] C. Coutanceau, P. Urchaga, S. Baranton, Electrochem. Commun. 22 (2012) 109–112.
[31] J. Solla-Gullon, F.J. Vidal-Iglesias, E. Herreo, J.M. Feliu, A. Aldaz, Electrochem. Commun. 8 (2006) 189–194.
[32] J. Solla-Gullon, V. Montiel, A. Aldaz, J. Clavillier, J. Electrochem. Soc. 150 (2003) E104–E109.
[33] Q. Xu, E. Kreidler, D.O. Wipf, T. He, J. Electrochem. Soc. 155 (2008) B228–B231.
[34] Y. Sugawara, A.P. Yadav, A. Nishikata, T. Tsuru, J. Electroanal. Chem. 662 (2011) 379–383.
[35] K. Hartl, M. Nesselberger, K.J.J. Mayrhofer, S. Kunz, F.F. Schweinberger, G.H. Kwon, M. Hanzlik, U. Heiz, M. Arenz, Electrochim. Acta 56 (2010) 810–816.
[36] L. Tang, B. Han, K. Persson, C. Friesen, T. He, K. Sieradzki, G. Ceder, J. Am. Chem. Soc. 132 (2010) 596–600.
[37] K.J.J. Mayrhofer, J.C. Meier, S.J. Ashton, G.K.H. Wiberg, F. Kraus, M. Hanzlik, M. Arenz, Electrochem. Commun. 10 (2008) 1144–1147.
[38] S. Stevanović, D. Tripković, V. Tripković, D. Minić, A. Gavrilović, A. Tripković, V.M. Jovanović, J. Phys. Chem. C 118 (2014) 278–289.
[39] F. Maillard, S. Schreier, M. Hanzlik, E.R. Savinova, S. Weinkauf, U. Stimming, Phys. Chem. Chem. Phys. 7 (2005) 385–393.
[40] A. Lopez-Cudero, J. Solla-Gullon, E. Herrero, A. Aldaz, J.M. Feliu, J. Electroanal. Chem. 644 (2010) 117–126.
[41] N.P. Lebedeva, M.T.M. Koper, E. Herrero, J.M. Feliu, R.A. van Santen, J. Electroanal. Chem. 487 (2000) 37–44.
[42] G. García, M.T.M. Koper, J. Am. Chem. Soc. 131 (2009) 5384–5385.
[43] G. García, M.T.M. Koper, Phys. Chem. Chem. Phys. 10 (2008) 3802–3811.
[44] J.W. Spendelow, G.Q. Lu, P.J.A. Kenis, A. Wieckowski, J. Electroanal. Chem. 568 (2004) 215–224.
[45] J. Solla-Gullon, F.J. Vidal-Iglesias, A. Lopez-Cudero, E. Garnier, J.M. Feliu, A. Aldaz, Phys. Chem. Chem. Phys. 10 (2008) 3689–3698.
[46] S. Park, Y. Xie, M. Weaver, Langmuir 18 (2002) 5792–5798.
[47] R.R. Adzic, A.V. Tripkovic, V.B. Vesovic, J. Electroanal. Chem. 204 (1986) 329–341.
[48] M. Arenz, K.J.J. Mayrhofer, V. Stamenkovic, B.B. Blizanac, T. Tomoyuki, P.N. Ross, N.M. Markovic, J. Am. Chem. Soc. 127 (2005) 6819–6829.
[49] A.A. Topalov, S. Cherevk, A.R. Zeradjanin, J.C. Meier, I. Katsounaros, K.J.J. Mayrhofer, Chem. Sci. 5 (2014) 631–638.
[50] S. Mitsushima, Y. Koizumi, S. Uzuka, K.I. Ota, Electrochim. Acta 54 (2008) 455–460.
[51] A.A. Topalov, I. Katsounaros, M. Auinger, S. Cherevko, J.C. Meier, S.O. Klemm, K.J.J. Mayrhofer, Angew. Chem. 51 (2012) 12613–12615.
[52] M. Fayette, J. Nutariya, N. Vasiljevic, N. Dimitrov, ACS Catal. 3 (2013) 1709–1718.
[53] X. Zhang, H.M. Galindo, H.F. Garces, P. Baker, X. Wang, U. Pasaogullari, S.L. Suib, T. Molter, J. Electrochem. Soc. 157 (2010) B409–B414.
[54] L. Tang, X. Li, R.C. Cammarata, C. Friesen, K. Sieradzki, J. Am. Chem. Soc. 132 (2010) 11722–11726.
[55] V. Komanicky, K.C. Chang, A. Menzel, N.M. Markovic, H. You, X. Wang, D. Mayers, J. Electrochem. Soc. 153 (2006) B446–B451.